Supporting information for:

Activation of Molecular Oxygen by a Molybdenum Complex for Catalytic Oxidation

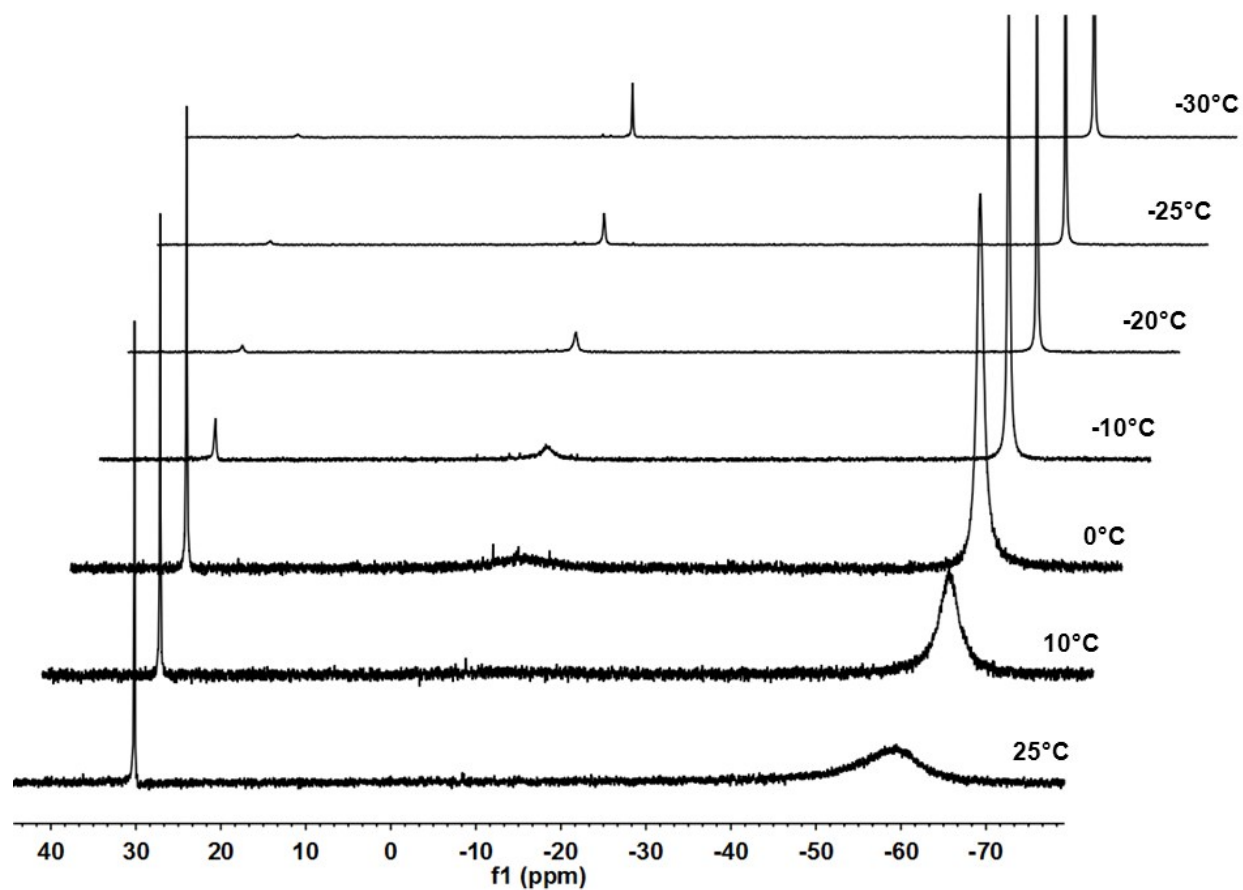Antoine Dupé,[‡a] Martina E. Judmaier,[‡a] Ferdinand Belaj[a], Klaus Zangger[b] and Nadia C. Mösch-Zanetti[*a]

[a]*Institute of Chemistry, University of Graz, Schubertstrasse 1, 8010 Graz, Austria*
*email: noadia.moesch@uni-graz.at*
[b]*Institute of Chemistry, University of Graz, Heinrichstrasse 28/II, 8010 Graz, Austria*

‡ These authors contributed equally to this work

Figure S 1: Low-temperature ^{31}P NMR spectrum of complex **2** with OPMe$_3$ and excess PMe$_3$ in toluene-d$_8$. The signal at -9.5 ppm is the signal corresponding to complex **2**. The signal at 30 ppm is the OPMe$_3$ and disappears upon precipitation of OPMe$_3$ at low temperature.
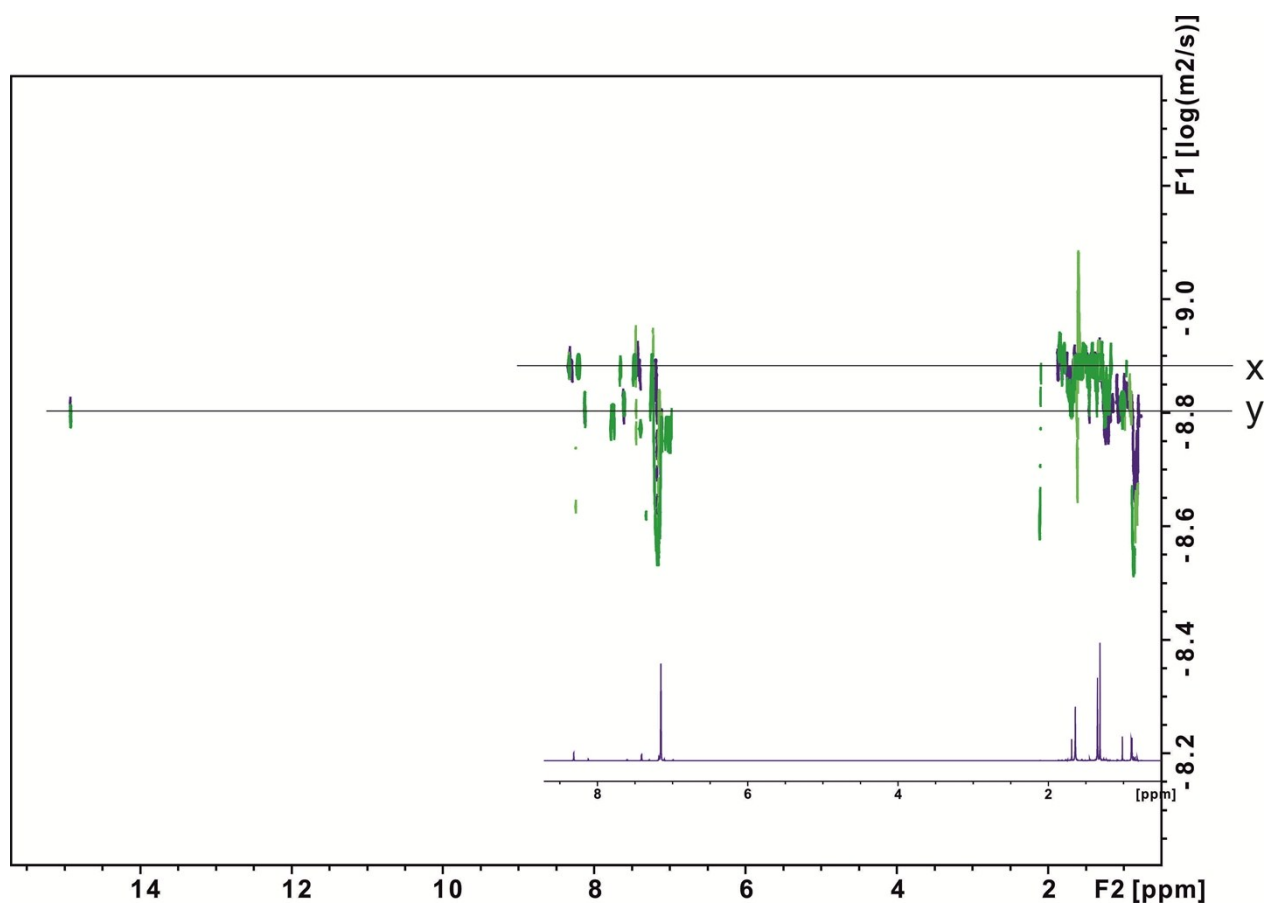
Figure S 2: Overlay of 2D DOSY spectra in benzene-d$_6$ at 298 K of complex **2** + free ligand (purple), complex **1** + complex **2** (light green) and complex **1** + complex **3** + free ligand (dark green). Mixtures were chosen to allow calculation of the relative size of the complexes in comparison to the free ligand. It also allows direct comparison of **2** and **3** to **1** from which we know the monomeric nature. The three complexes **1**, **2** and **3** have the same diffusion coefficient D= -8.878 log (m^2/s) indicated by the **x** line. The free ligand has a diffusion coefficient D= -8.805 log (m^2/s) indicated by the **y** line. A 1D ^{1}H spectrum of complex **2** in benzene-d$_6$ is shown in the inset. Based on the Stokes-Einstein equation, the relative hydrodynamic radii of two components are related to the diffusion coefficients by $D_1/D_2=r_2/r_1$. Therefore, the experimental diffusions coefficients of the complexes and free ligand correspond to relative hydrodynamic radii of 1.18:1.
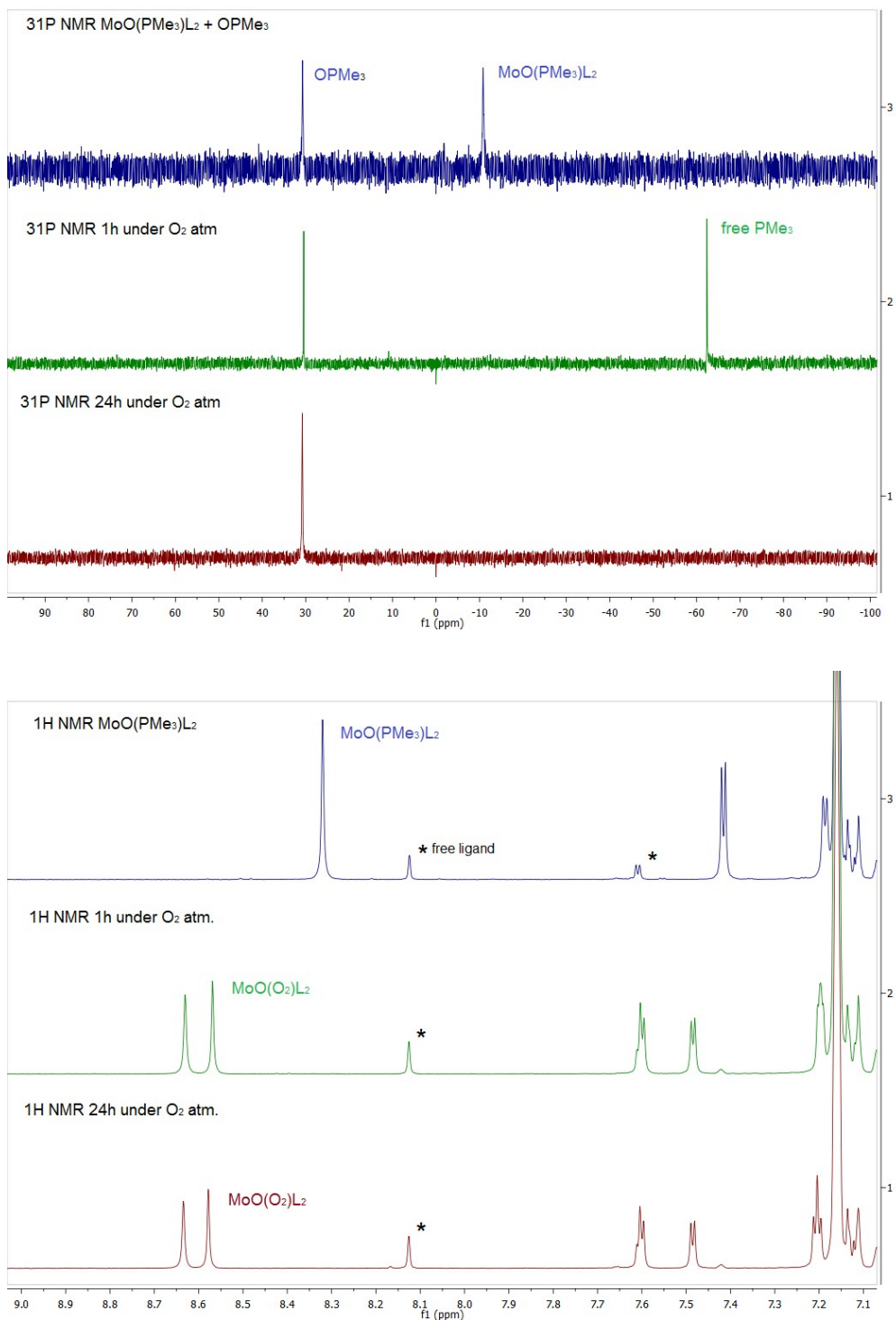
Figure S 3: ^{31}P and ^{1}H NMR spectra in benzene-d_6 of the re-oxidation of the complex [MoO(PMe$_3$)L$_2$] **2** with O$_2$. The PMe$_3$ molecule bound to Mo in complex **2** is initially released when the complex reacts with O$_2$ to form the oxo-peroxo complex **4**, then converted to OPMe$_3$.
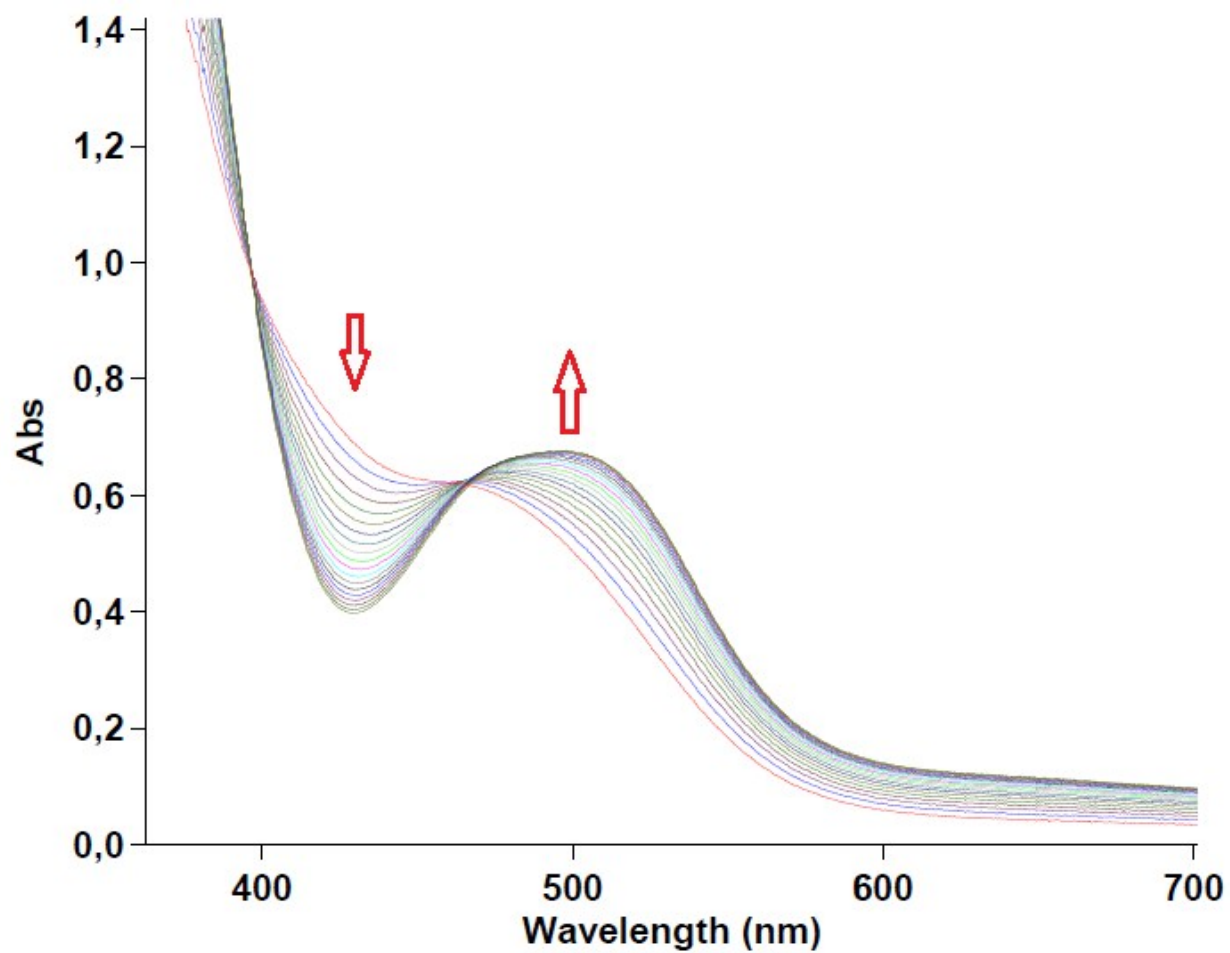
Figure S 4: UV-Vis spectra of the reaction of **1** + 100 equiv PMe$_3$ in toluene at room temperature from t = 0 to 15 minutes.

Oxygen Atom Transfer reactivity of [MoO(O$_2$)L$_2$] (4). [MoO(O$_2$)L$_2$] (25 mg, 0.035 mmol, 1 equiv) was dissolved in dry benzene-d$_6$ under inert conditions in a Young NMR tube. 2 equivalent PMe$_3$ (8 μL, 0.07 mmol) was added using a micropipette. The OAT reaction was monitored by ^{1}H and ^{31}P NMR spectroscopy.
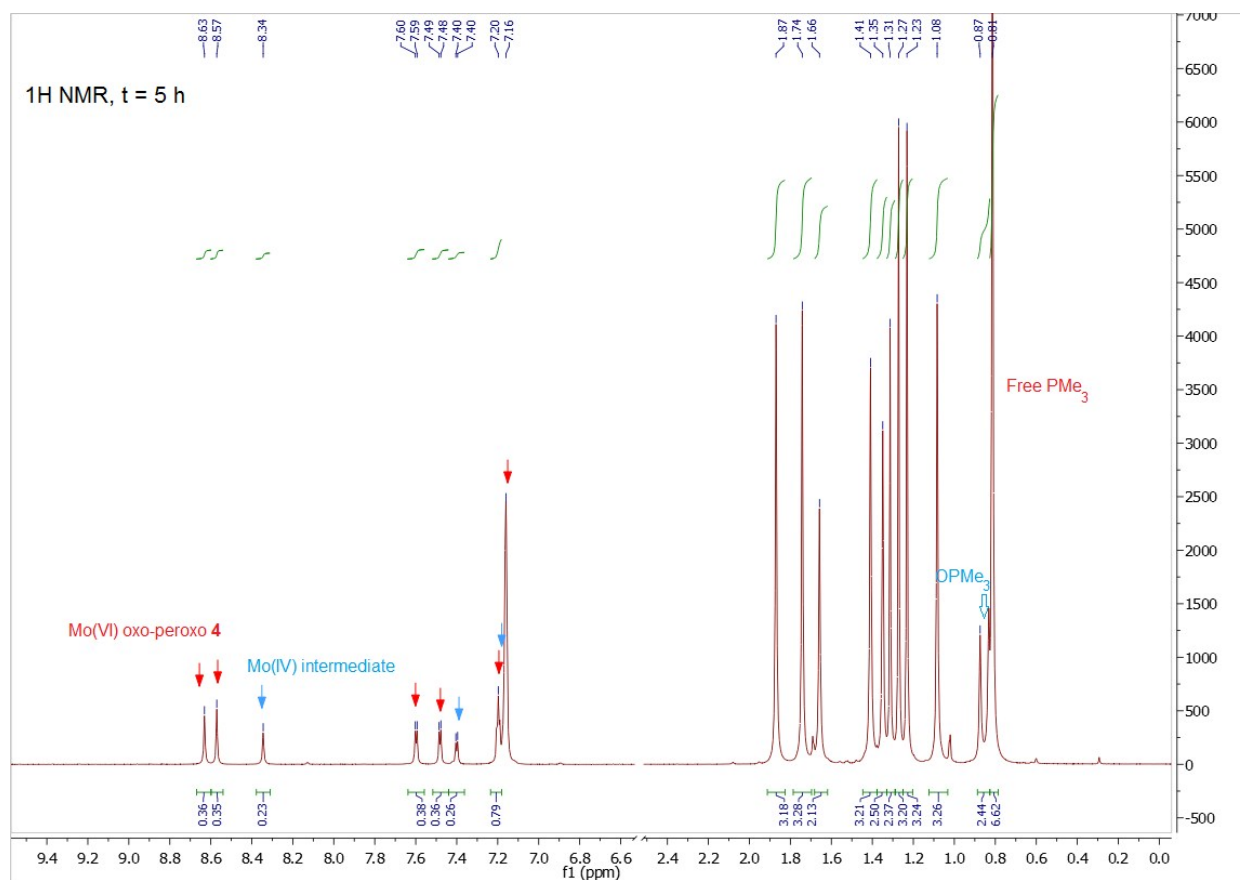
Figure S 5: ^{1}H NMR spectrum at t = 5 h of the reaction of molybdenum oxo-peroxo complex **4** with 2 equiv PMe$_3$ in benzene-d$_6$ under O$_2$ exclusion.
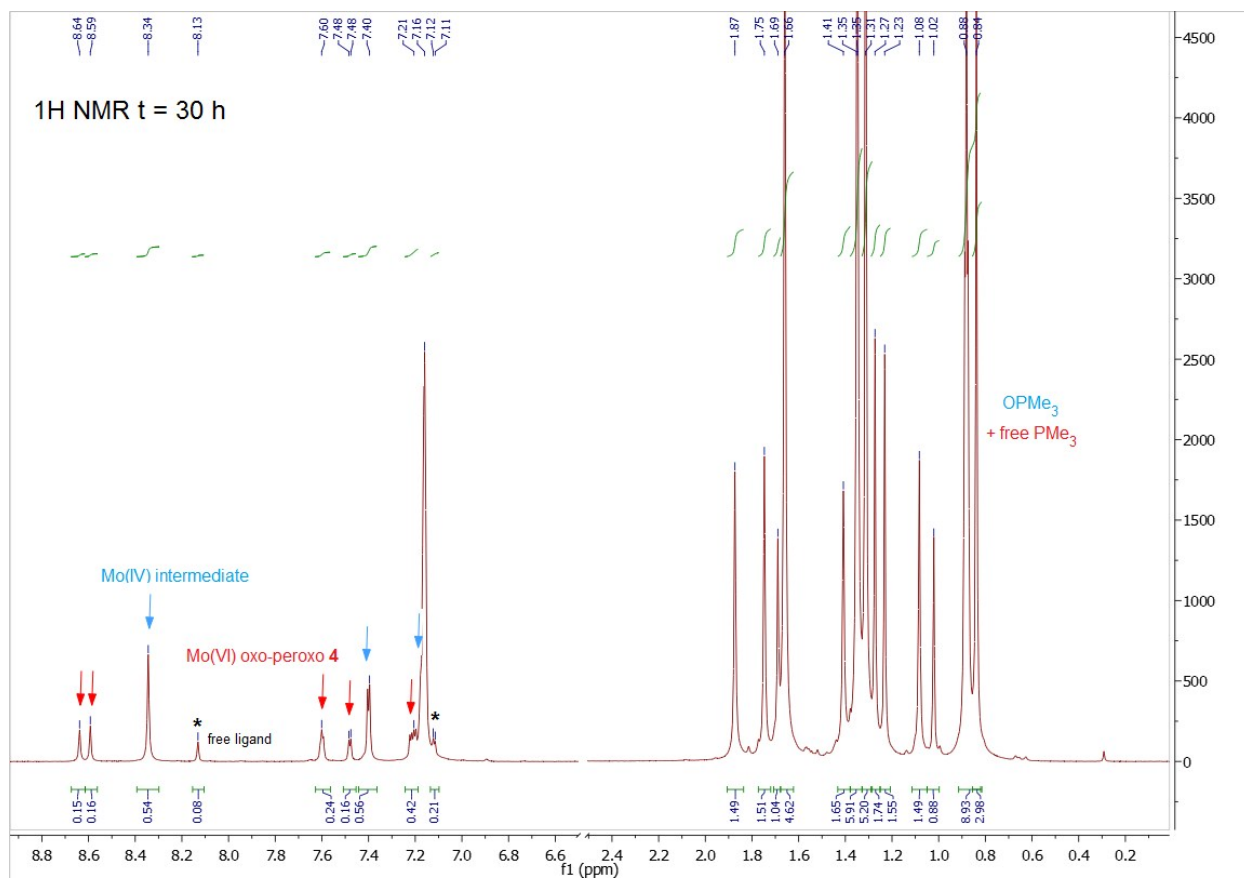
Figure S 6: ^1H NMR spectrum at t = 30 h of the reaction of molybdenum oxo-peroxo complex **4** with 2 equiv PMe$_3$ in benzene-d$_6$ under O$_2$ exclusion.

Catalytic oxidation of trimethylphosphine. [MoO$_2$L$_2$] (complex 1, 10 mg, 14 μmol) was placed in a Schlenk flask in the glovebox. The Schlenk flask was evacuated then refilled with dry O$_2$. Dry benzene-d$_6$ (2 mL) and trimethylphosphine (108 mg, 0.15 μL, 1.4 mmol, 100 equiv) were added and the reaction was left to stir under O$_2$ atmosphere for 24 h. The reaction was monitored by ^1H and ^{31}P NMR at t= 4 h, 20 h and 24 h. After removal of the solvent, the mass balance was calculated and the yield of OPMe$_3$ confirmed by integration of the signals in the ^1H NMR spectrum at t= 24 h (yield = 19 %).
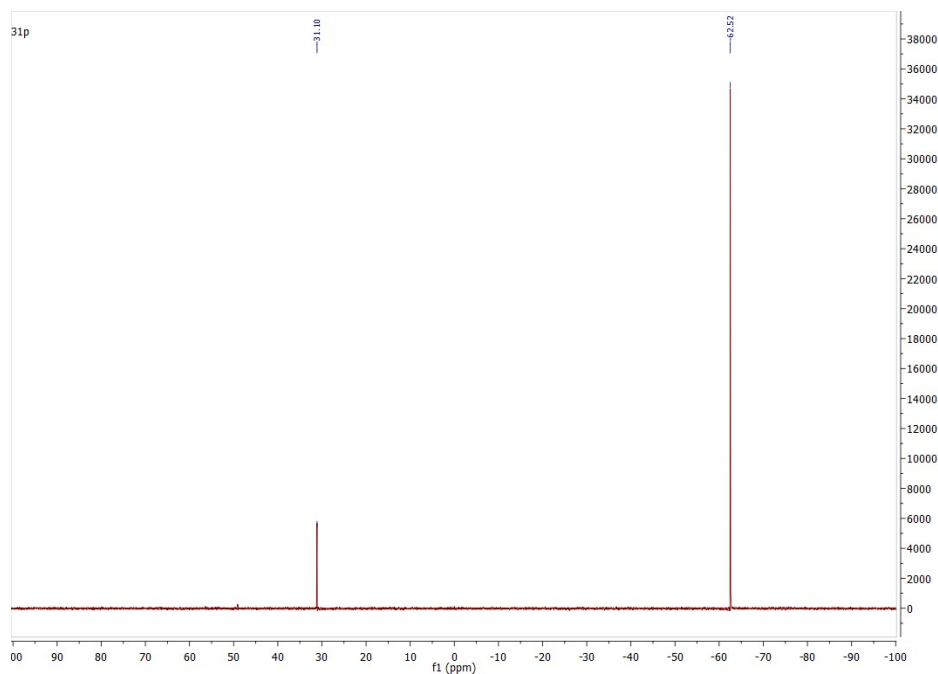
Figure S 7: ^{31}P NMR spectrum at t = 24 h of the catalytic oxidation of PMe$_3$ under O$_2$ atmosphere using 1 mol-% of complex **1.**
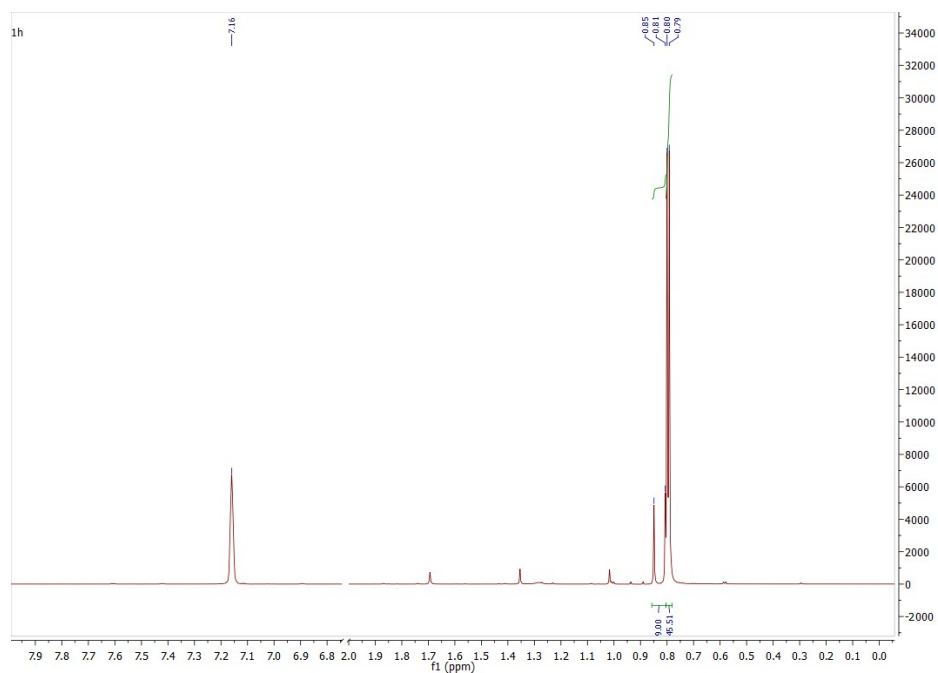
Figure S 8: ^1H NMR spectrum at t = 24 h of the catalytic oxidation of PMe$_3$ under O$_2$ atmosphere using 1 mol-% of complex **1**. The doublet at 0.80 ppm is free PMe$_3$, the doublet at 0.83 ppm is OPMe$_3$. Other peaks arise from free ligand.

To confirm the stability of PMe$_3$ under O$_2$ atmosphere, a blank experiment was performed. A Schlenk flask was evacuated then refilled with dry O$_2$. Dry benzene-d$_6$ (2 mL) and trimethylphosphine (108 mg, 0.15 μL, 1.4 mmol, 100 equiv) were added and the reaction was left to stir under O$_2$ atmosphere for 24 h. The reaction was monitored by ^{1}H and ^{31}P NMR at t= 4 h, 20 h and 24 h. at t = 24 h, a signal for OPMe$_3$ could be observed in the ^{1}H NMR (1% yield) but no signal was observed in ^{31}P NMR. After 24 h, the solvent and free PMe$_3$ were evaporated, no solid OPMe$_3$ could be isolated.
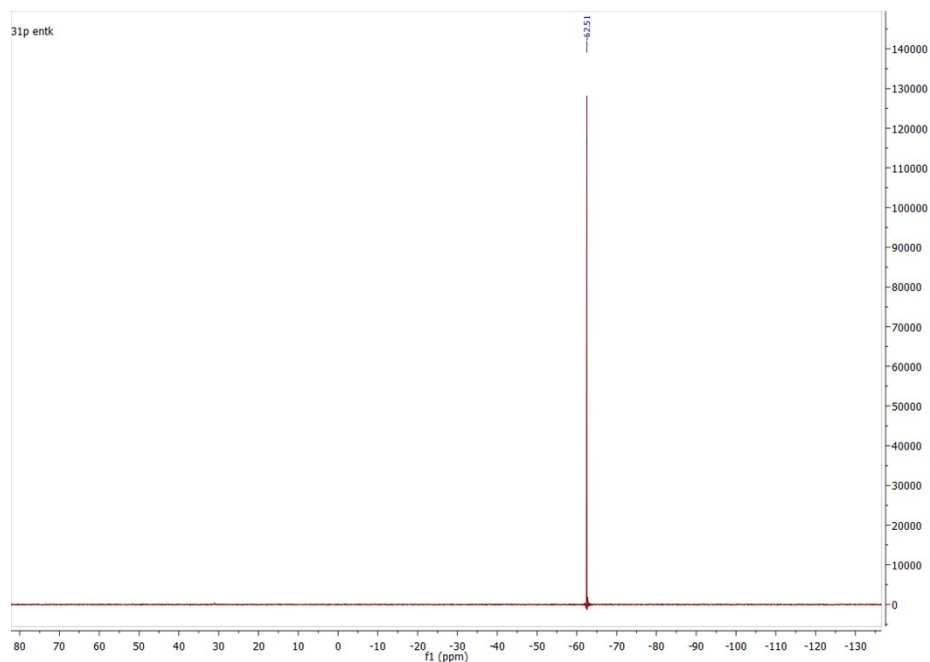
Figure S 9: ^{31}P NMR spectrum at t = 24 h of the catalytic oxidation of PMe$_3$ under O$_2$ atmosphere in the absence of complex **1.**
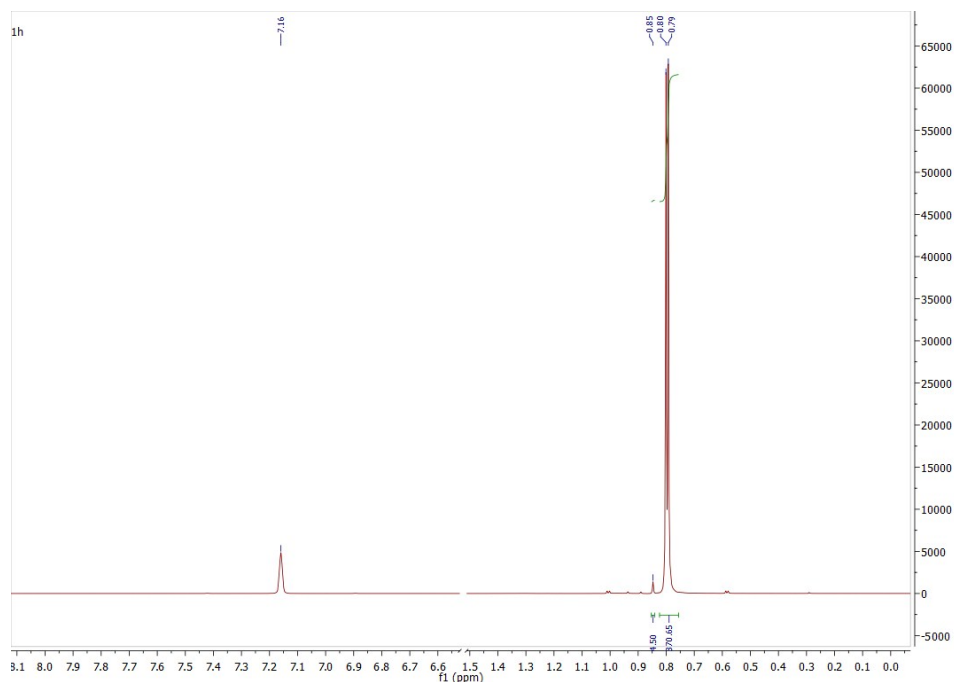
Figure S 10: ^{1}H NMR spectrum at t = 24 h of the catalytic oxidation of PMe$_3$ under O$_2$ atmosphere in the absence of complex **1.**

X-ray structure determination

For X-ray structure analyses the crystals were mounted onto the tip of glass fiber and data collection was performed at 100 K using graphite monochromated MoK$_\alpha$ radiation (λ = 0.71073Å) with a BRUKER-AXS SMART APEX II diffractometer equipped with a CCD detector. Essential details of the crystal-data and structure refinements for compounds **1** and **4** are summarized in Table 1. Crystallographic data for the structures of compounds **1** and **4** have been deposited with the Cambridge Crystallographic Data Center [CCDC-1413968 for **1**, CCDC-1413969 for **4**]. These data can be obtained free of charge from The Cambridge Crystallographic Data Centre via www.ccdc.cam.ac.uk/data_request/cif.

Crystal Structure Determination of 1. The structure was solved by direct methods (SHELXS-97) and refined by full-matrix least-squares techniques against F^2 (SHELXL-2014/6). The non-

hydrogen atoms were refined with anisotropic displacement parameters without any constraints. The H atoms of the phenyl rings as well as the H atoms bonded to the C atom of a C=N double bond were put at the external bisectors of the C–C–X angles at C–H distances of 0.95Å and common isotropic displacement parameters were refined for these H atoms of the same ligand. The H atoms of the methyl groups were refined with common isotropic displacement parameters for the H atoms of the same *tert*-butyl group and idealized geometries with tetrahedral angles, enabling rotation around the C–C bonds, and C–H distances of 0.98Å.

Crystal Structure Determination of 4. The structure could be solved (SHELXS-97) by interpretation of the patterson map (second solution) in the non-centrosymmetric space group C 2, but not in centrosymmetric C 2/c. After completion of the molecule an inversion center could be detected and the structure was refined by full-matrix least-squares techniques against F2 (SHELXL-2014/6) in the centric space group C 2/c after an appropriate shift of the origin. A void of approx. 188Å3 is occupied by a THF molecule disordered over two orientations lying near a center of symmetry or by a n-pentane molecule at the inversion center. The ratio of the refined occupation factors is 0.768(6) to 0.232(6). The non-hydrogen atoms of the solvent molecules were refined with isotropic displacement parameters with some restraints. The H atoms of the solvent molecules were included at calculated positions with their isotropic displacement parameters fixed to 1.2 times U_{eq} of the C atom they are bonded to. The non-hydrogen atoms of the metal complex were refined with anisotropic displacement parameters without any constraints. The H atoms of the phenyl rings were put at the external bisectors of the C–C–C angles at C–H distances of 0.95Å and common isotropic displacement parameters were refined for the H atoms of the same ring. The H atoms H10 and H30 were put at the external bisector of the C–C–C angle at a C–H distance of 0.95Å but the individual isotropic displacement parameters were free to refine. The H atoms of the methyl groups were refined with common isotropic displacement parameters for the H atoms of the same group and idealized geometries with tetrahedral angles, enabling rotation around the C–C bond, and C–H distances of 0.98Å.

Table S 1: Crystallographic data and structure refinements for complexes **1** and **4**

	1	**4**
empirical formula	$C_{38}H_{60}MoN_2O_4$	$2\ MoO_5N_2C_{38}H_{60} \cdot x\ C_4H_8O \cdot (1-x)\ C_5H_{12}$; $x = 0.786(6)$
formula weight	704.82	1513.75
crystal description	plate, red	block, red
crystal size (mm)	0.27 x 0.17 x 0.05mm	0.32 x 0.25 x 0.25
crystal system, space group	monoclinic, P 21/n	monoclinic, C 2/c
Unit cell dimensions, a (Å)	10.3863(4)	24.3085(13)
b (Å)	11.4627(5)	15.8102(8)
c (Å)	33.1945(13)	20.8035(11)
α (deg)	90	90
ß (deg)	98.6499(17)	94.112(2)
γ (deg)	90	90
volume (Å^3)	3907.0(3)	7974.7(7)
Z, Calculated density (gcm^{-3})	4, 1.198	4, 1.261
F(000)	1504	3233.9
linear absorption coefficient µ (mm^{-1})	0.373	0.373
absorption correction	semi-empirical from equiv.	semi-empirical from equiv.
temperature (K)	100	100
wavelength (MoK$_\alpha$) (Å)	0.71073	0.71073
theta range for data collection (deg)	2.46 to 28.45	1.79 to 30.00
limiting indices	$-12 \leq h \leq 12$	$-34 \leq h \leq 29$
	$-5 \leq k \leq 14$	$-22 \leq k \leq 22$
	$-40 \leq l \leq 40$	$-29 \leq l \leq 29$
reflections collected / unique	26791 / 7661	46647 / 11648
reflections with I > 2σ(I)	5550	10882
R(int), R(sigma)	0.0549, 0.0723	0.0187, 0.0148
completeness to theta max.	0.999	0.999
refinement method	full matrix least squares on F^2	full matrix least squares on F^2
data / restraints / parameters	7661 / 432 / 0	11648 / 486 / 12
goodness-of-fit on F^2	1.107	1.100
final R1[a] wR2[b] [I>2σ(I)]	R1 = 0.0585	R1 = 0.0277
	wR2 = 0.1401	wR2 = 0.0689
R indices (all data)	R1 = 0.0869	R1 = 0.0304
	wR2 = 0.1507	wR2 = 0.0709
largest diff. peak and hole (eÅ-3)	1.484 and -2.767	1.283 and -0.599
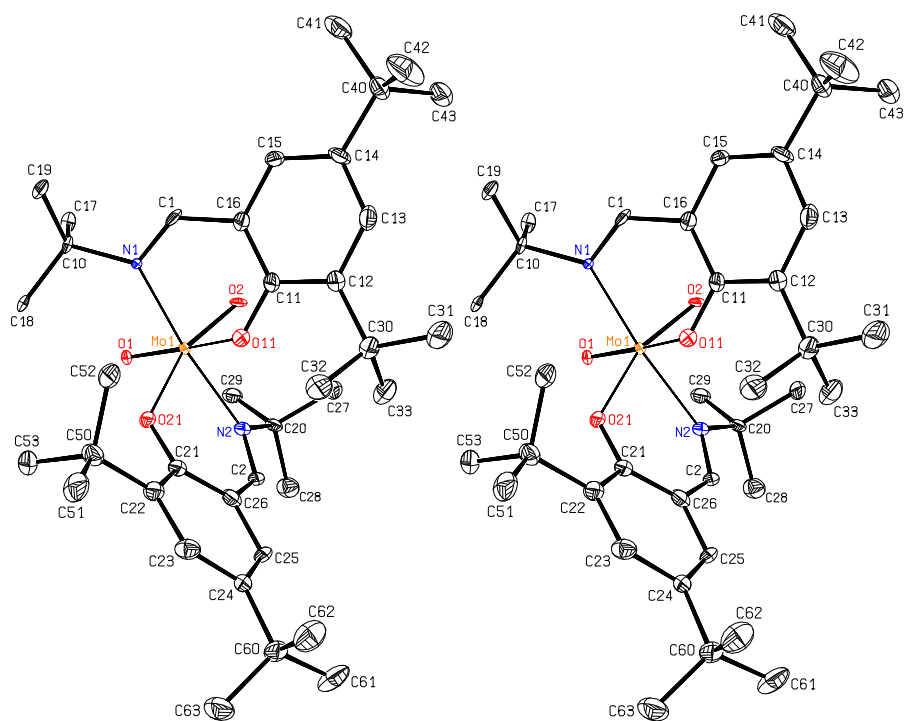
Figure S 11: Stereoscopic ORTEP plot of **1** showing the atomic numbering scheme. The probability ellipsoids are drawn at the 50% probability level. The H atoms were omitted for clarity reasons.
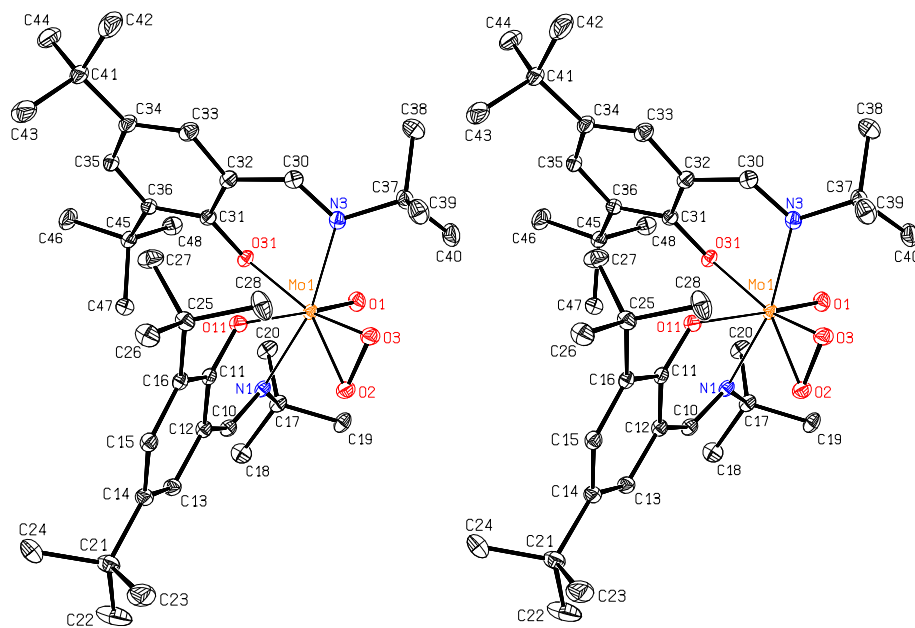
Figure S 12: Stereoscopic ORTEP plot of **4** showing the atomic numbering scheme. The probability ellipsoids are drawn at the 50% probability level. The H atoms were omitted for clarity reasons.